Supporting Information

Dynamically reconfigurable artificial synapses transistors with organic heterojunction for multifunctional neuromorphic applications

Tao Wang,[a] Minghao Zhang,[a] Chaoyou Xu,[b] Fengxu Guo,[b] Yiran Wang,[a] Jie Su,*[b] and Ting Xu*[b]

[a]College of Physics Science. Qingdao University. Qingdao 266071, P. R. China

[b]College of Electronic and Information Engineering. Qingdao University. Qingdao 266071, P. R. China. Email: xuting@qdu.edu.cn

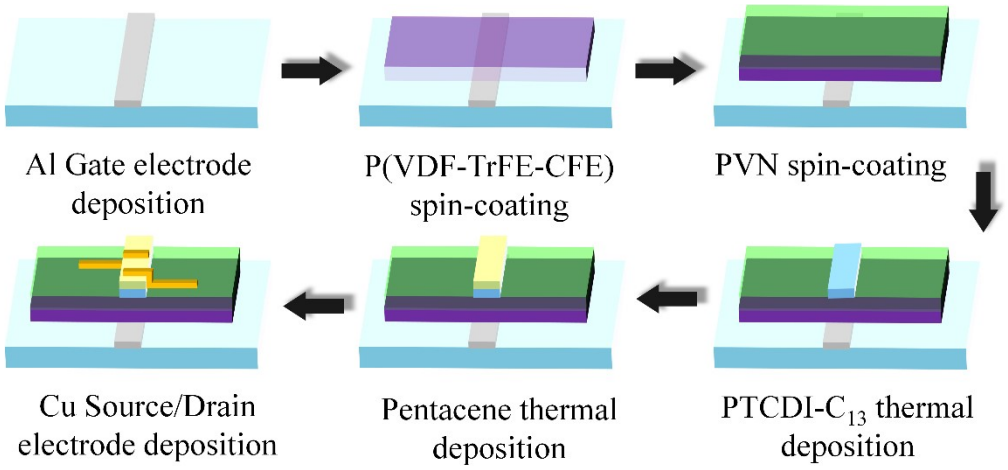

Fig. S1. Illustration of the EOHST fabrication process.

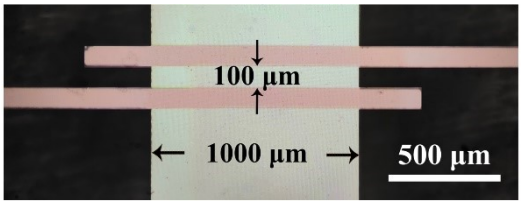

Fig. S2. Optical microscopy image of the EOHST and the diagram of single device.

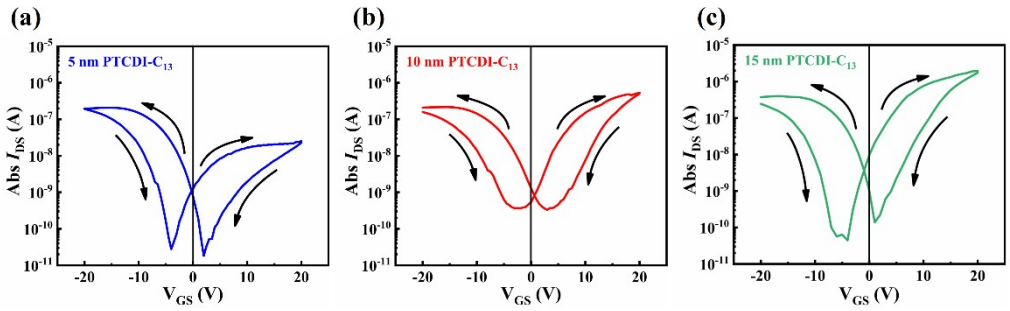

Fig. S3. The I_{DS}-V_{GS} curves of different PTCDI-C_{13} thickness layer devices.

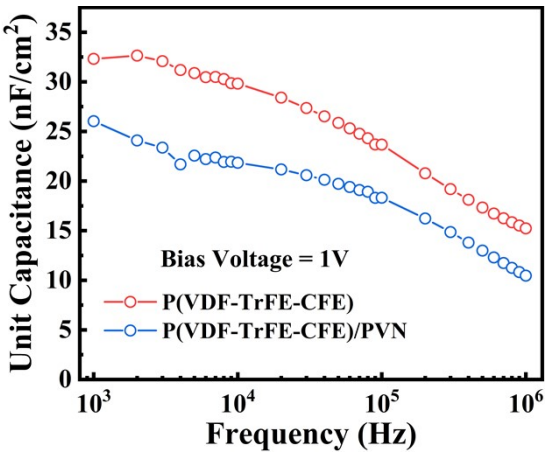

Fig. S4. The capacitances of the P(VDF-TrFE-CFE) and P(VDF-TrFE-CFE)/PVN composite gate dielectric layers, respectively.

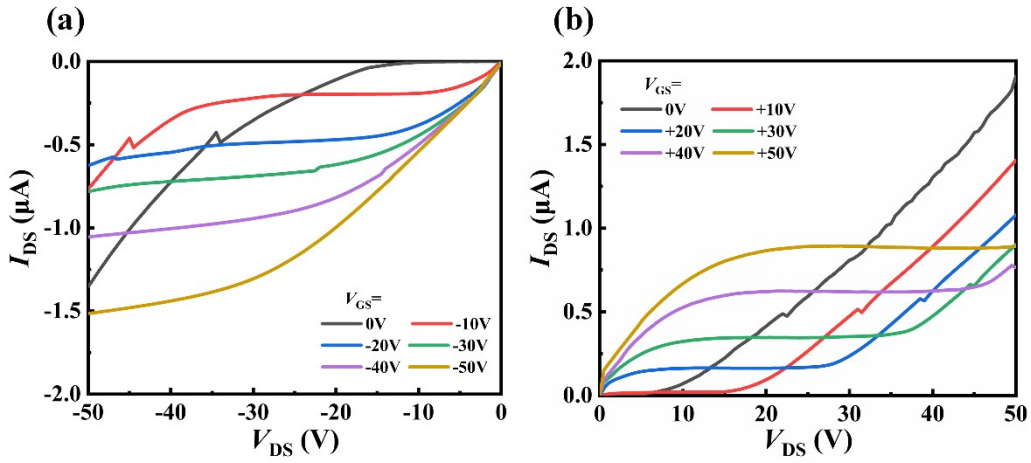

Fig. S5. (a) Output characteristics of hole-enhancement mode. (b) Output characteristics of electron-enhancement modes.

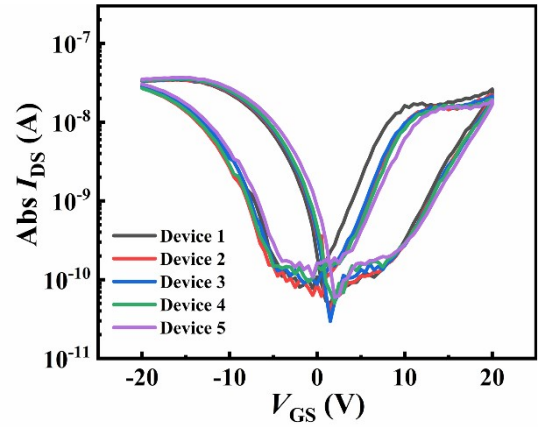

Fig. S6. The I_{DS}-V_{GS} curves of five single devices.

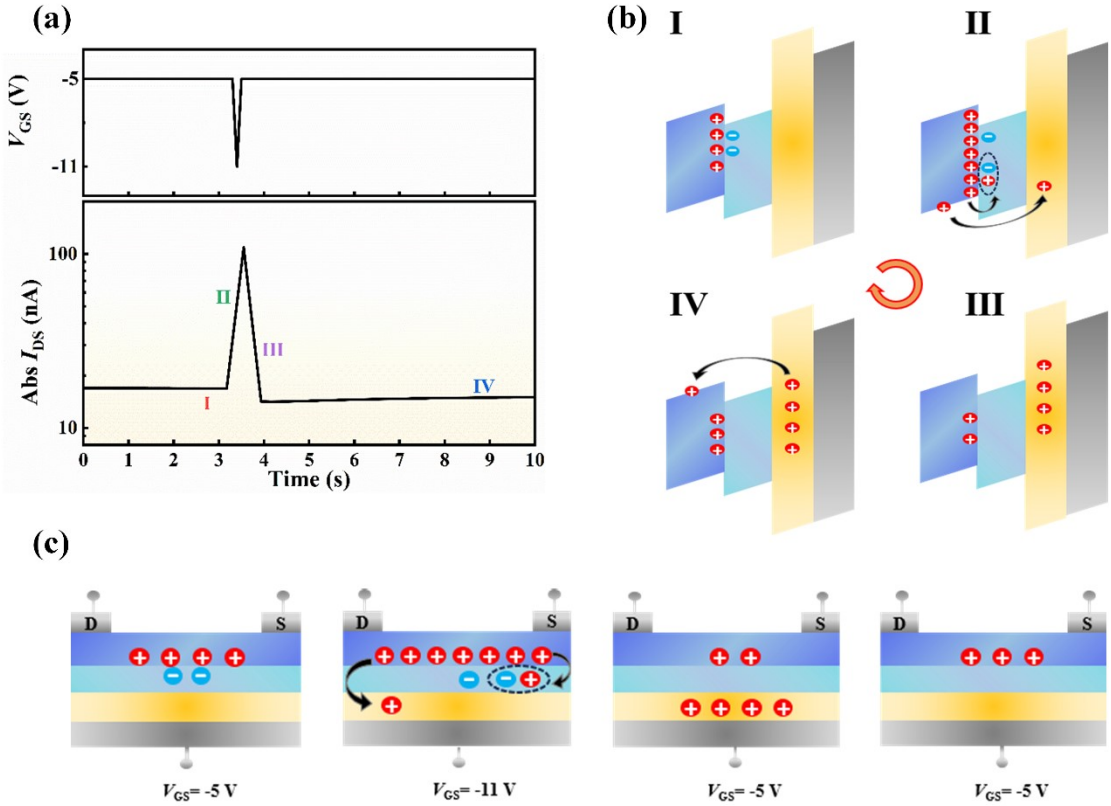

Fig. S7. (a) PSC with a four-stage variation characteristic under a positive gate pulse in the excitatory mode. The PSC was divided into Stages I, II, III, and IV. (b) Schematic illustration of the work mechanism and band diagram from Stages I to IV. (c) An intuitive illustration of the charge-trap state and the charge distribution in channels for depression behavior in the excitatory mode.

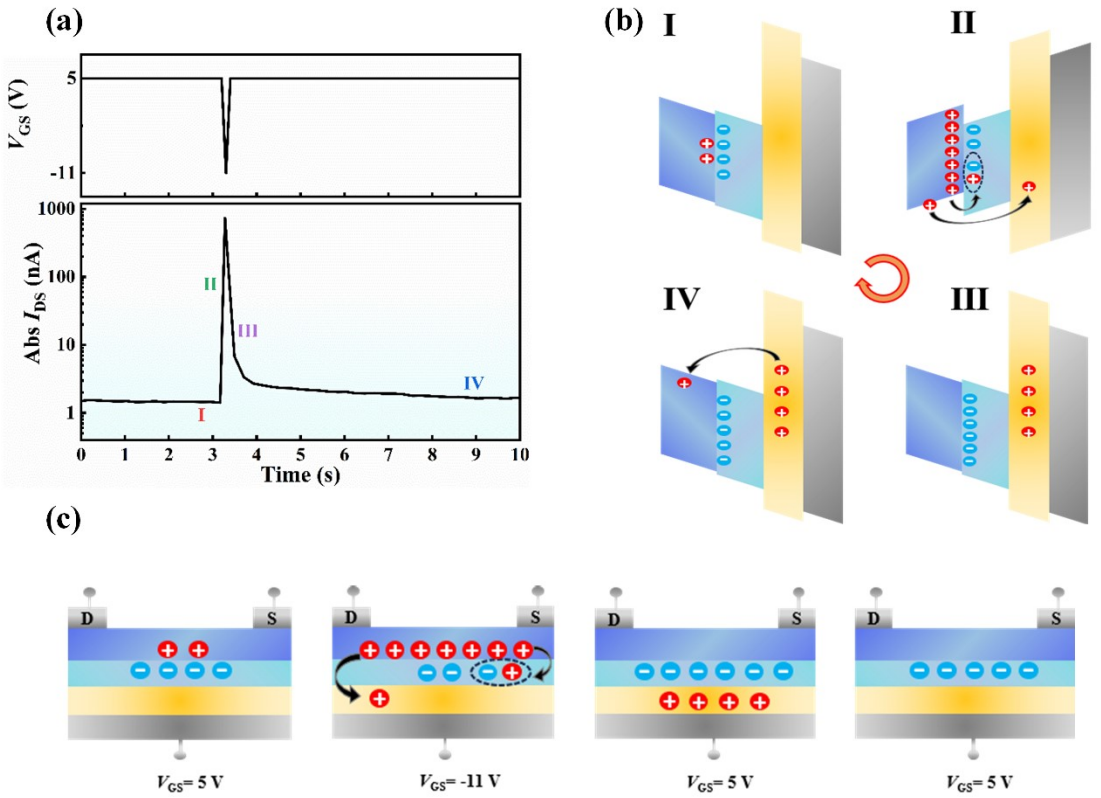

Fig. S8. (a) PSC with a four-stage variation characteristic under a negative gate pulse in the inhibitory mode. The PSC was divided into Stages I, II, III, and IV. (b) Schematic illustration of the work mechanism and band diagram from Stages I to IV. (c) An intuitive illustration of the charge-trap state and the charge distribution in channels for potentiation behavior in the inhibitory mode.

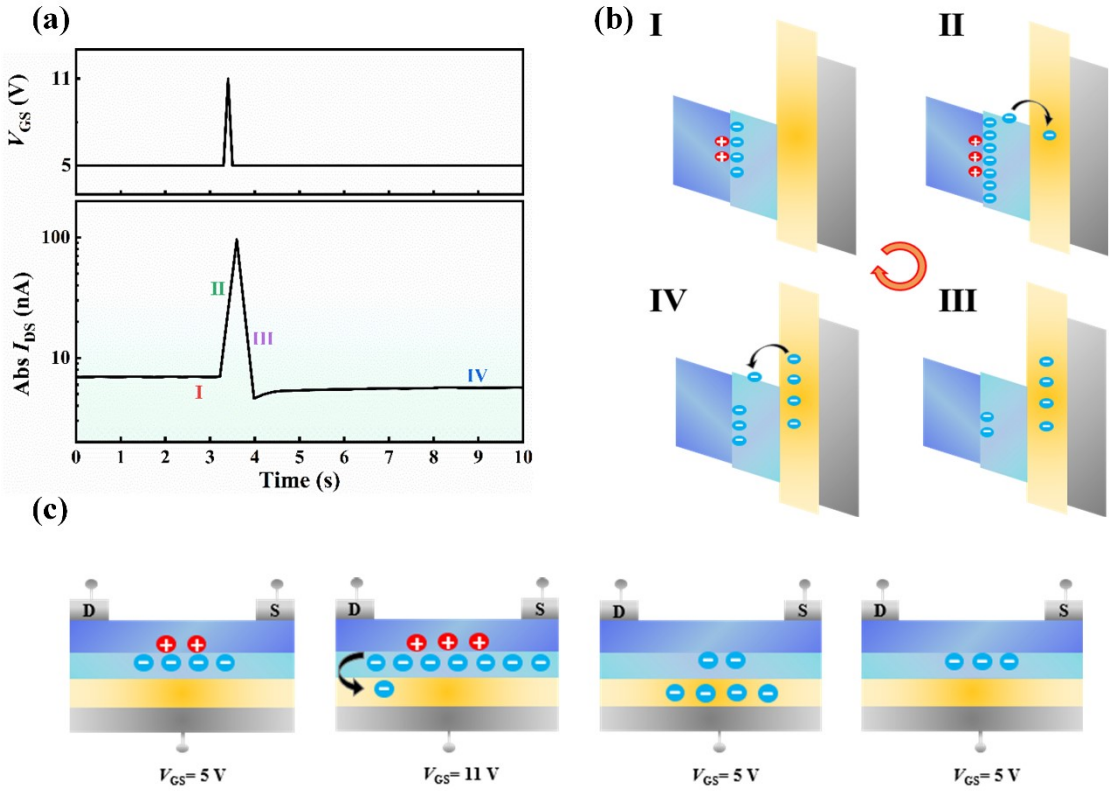

Fig. S9. (a) PSC with a four-stage variation characteristic under a positive gate pulse in the inhibitory mode. The PSC was divided into Stages I, II, III, and IV. (b) Schematic illustration of the work mechanism and band diagram from Stages I to IV. (c) An intuitive illustration of the charge-trap state and the charge distribution in channels for depression behavior in the inhibitory mode.

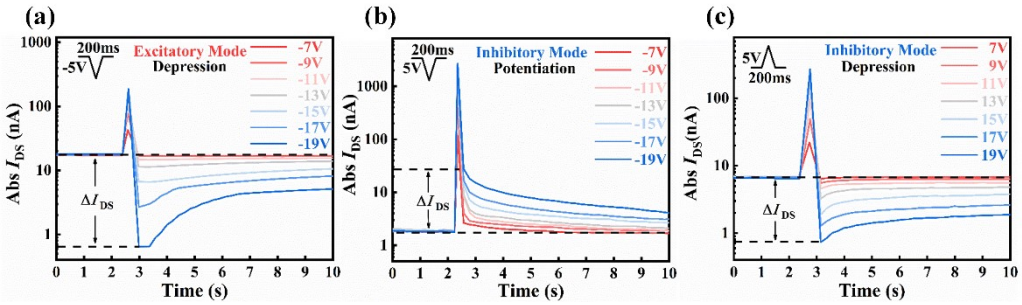

Fig. S10. (a) Depression behaviors under different amplitude pulses in excitatory mode. (b) Potentiation and (c) depression behaviors under different amplitude pulses in inhibitory mod.

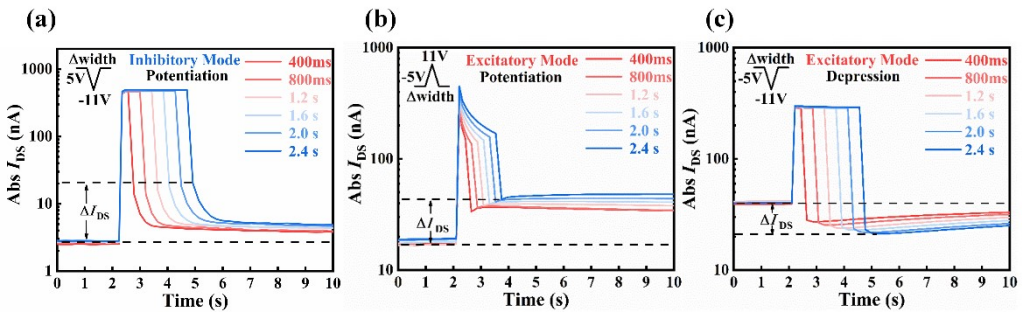

Fig. S11. (a) Potentiation behaviors under different width pulses in inhibitory mode. (b) Potentiation and (c) depression behaviors under different width pulses in excitatory mode.

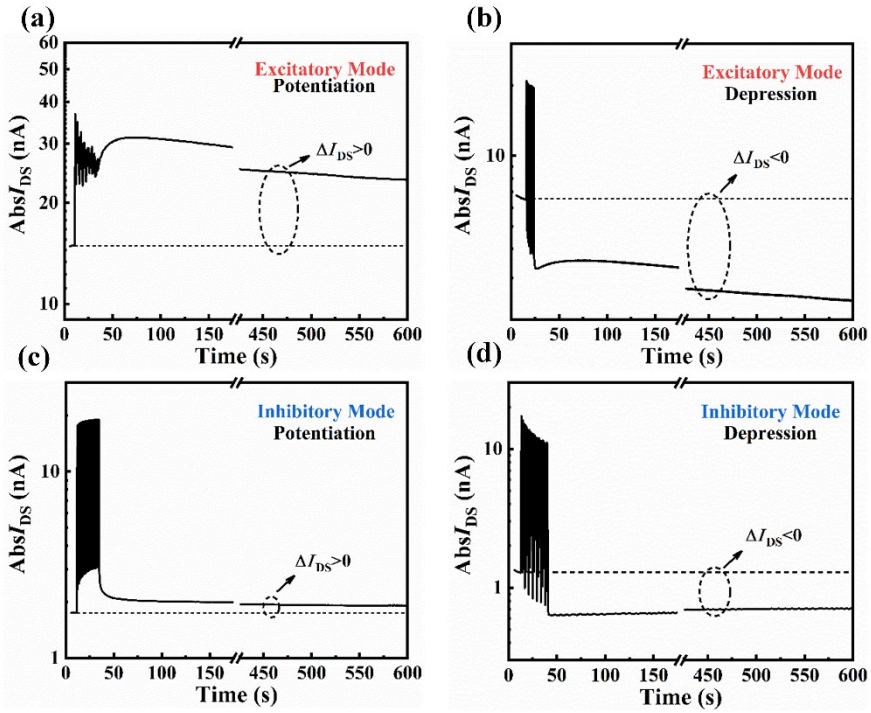

Fig. S12. (a) Depression (baseline voltage = -5V, pulse voltage = -11 V, pulse width = 200 ms, number of pulses = 10) and (b) potentiation (baseline voltage = -5V, pulse voltage = +11 V, pulse width = 200 ms, number of pulses = 10) behavior in the excitatory mode for LTP. (c) Depression (baseline voltage = +5V, pulse voltage = +11 V, pulse width = 200 ms, number of pulses = 10) and (d) potentiation (baseline voltage = +5V, pulse voltage = -11 V, pulse width = 200 ms, number of pulses = 10) behavior in the inhibitory mode for LTP.

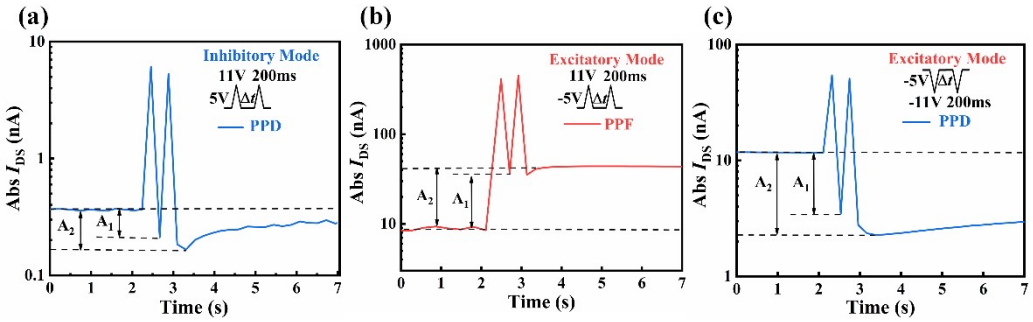

Fig. S13. (a) PPD behavior in inhibitory mode. (b) PPF behavior in excitatory mode. (c) PPD behavior in excitatory mode.

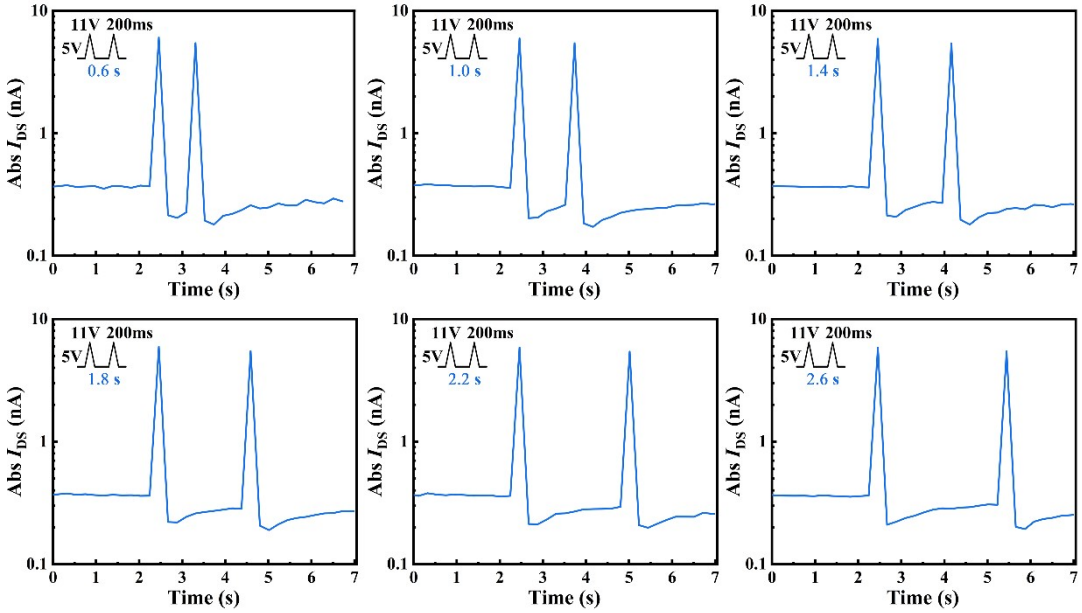

Fig. S14. The PPD behavior triggered by a pair of presynaptic pluses (with a baseline voltage of +5 V, pulse voltage of 11 V, pulse width of 200 ms).

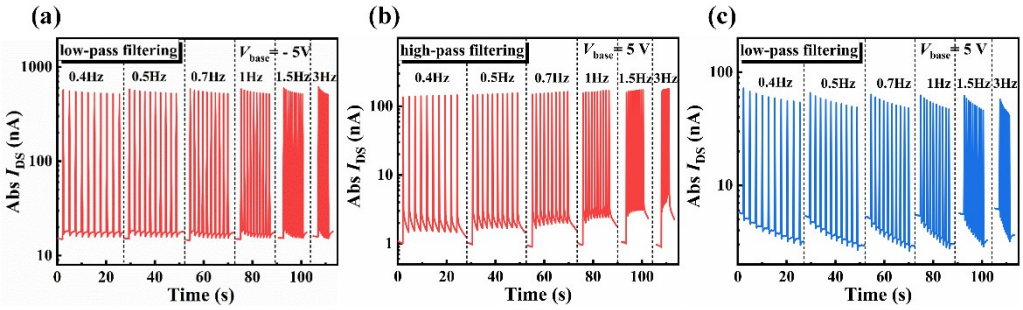

Fig. S15. (a) Potentiation behaviors induced by trains of 10 pulses at varying frequencies in excitatory mode. (b) Potentiation and (c) depression behaviors induced by trains of 10 pulses at varying frequencies in inhibitory mode.

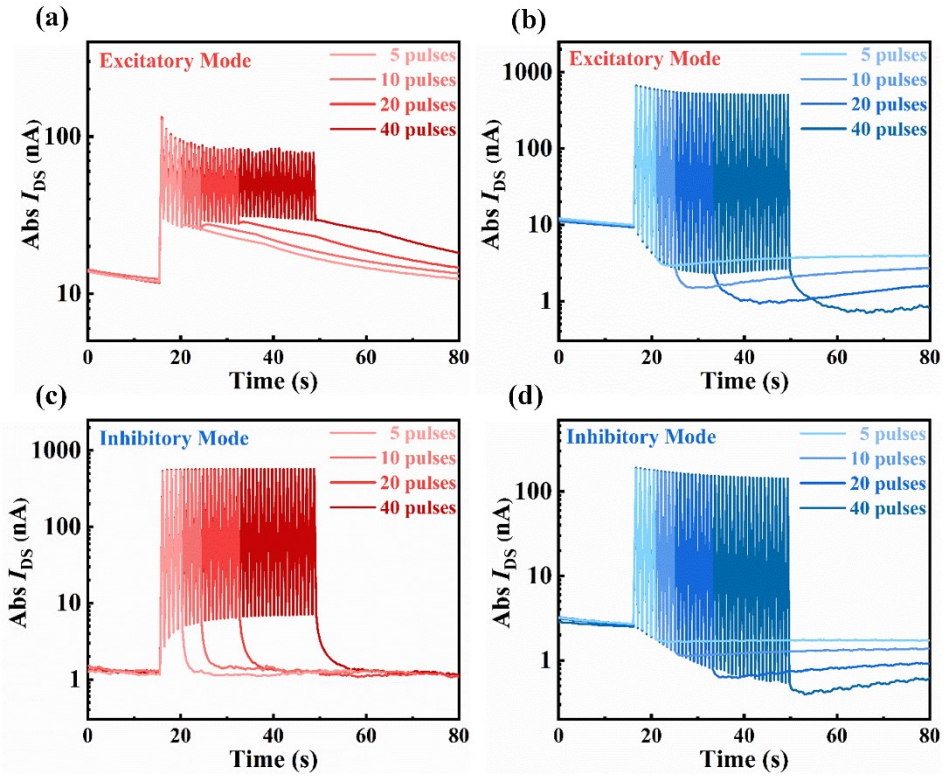

Fig. S16. SNDP under different numbers by (a) positive and (b) negative gate pulses in the excitatory mode. SNDP under different numbers by (a) negative and (b) positive gate pulses in the inhibitory mode.

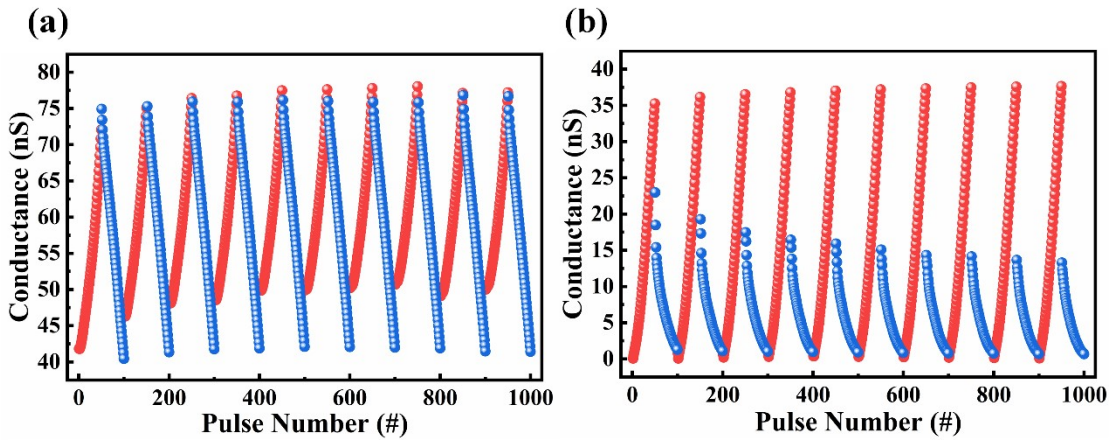

Fig. S17. Repeatability of long-term potentiation and depression in (a) excitatory mode and (b) inhibitory mode.

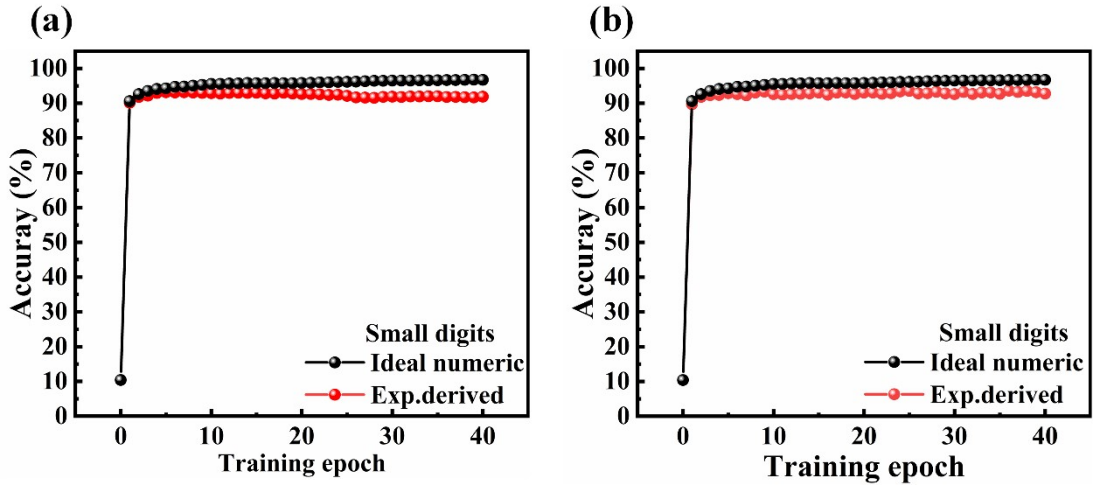

Fig. S18. The recognition accuracy evolution with training epochs for 8× 8 pixels handwritten digit image in (a) excitatory mode and (b) inhibitory mode.

Table S1. EOHST electrical characteristics for the PTCDI-C_{13} films with different film thicknesses devices.

	p-channel EOHST			n-channel EOHST		
	μ_h [$cm^2V^{-1}s^{-1}$]	I_{on}/I_{off} ratio	V_{th} [V]	μ_e [$cm^2V^{-1}s^{-1}$]	I_{on}/I_{off} ratio	V_{th} [V]
5 nm PTCDI-C_{13}	0.017±0.005	(4.05±2.58)×10^3	-2.5±1.061	~0.001	(0.27±0.03)×10^3	2.125±1.139
10 nm PTCDI-C_{13}	0.028±0.024	(0.97±0.73)×10^3	-3.3±1.03	0.039±0.016	(3.66±1.96)×10^3	2.3±1.078
15 nm PTCDI-C_{13}	0.017±0.006	(1.03±0.29)×10^3	-2.9±0.917	0.115±0.033	(7.26±0.83)×10^3	2.3±1.631

Table S2. Comparison of the comprehensive performance (On/off ratio, highest/lowest conductance ratio, potentiation and depression states, nonlinearity and accuracy) with other bipolar artificial neural devices.

Device structure	On/off ratio	Highest/Lowest conductance ratio	P/D states	Nonlinearity	Accuracy	Reference
WSe_2/h-BN/$MoTe_2$	10^8	30	57	2/-1.5 -0.3/-0.45	92%	[1]
MoS_2/P3HT NWs	--	15	30	--	86.6%	[2]
MoS_2/P(VDF-TrFE)	10^6	6	100	3	88%	[3]
P3HT/PEO/PMMA/TiO_2	--	3	30	--	93%	[4]
Ti_3C_2TX/TiO_2/MXene	10	10	100	--	90%	[5]
WSe_2/P(VDF-TrFE)	10^6	30	70	−2.8/1.46 0.56/−1.23	--	[6]
SnO:B	10^3	2	20	−3/1.6 1.5/−3.3	90%	[7]
Pentacene/ PTCDI-C_{13}/ PVN/ P(VDF-TrFE-CFE)	10^3	35	50	0.044/0.007 0.038/0.87	87.5%	This work

Supplementary Notes

Note 1: The concept and the importance of "dynamic reconfiguration" in the biological synapse

Dynamic reconfiguration, embodied in neuroscience as metaplasticity, or the plasticity of synaptic plasticity, is defined as "neural activity at one point in time can change cells or synapses such that their ability to exhibit LTP or LTD after a later bout of activity is altered".[8] Some neuromodulators, which can be viewed as neural activity at one point in time, result in changes in the ability of a cell or synapse to exhibit LTP or LTD afterward. Thus, the mechanism of dynamic reconfiguration can be explained by the fact that certain neuromodulators activate a sustained effect, which regulates synaptic plasticity. For example, NMDA can lead to "repetitive activation of NMDA receptors", which ultimately modulates subsequent LTP. Once NMDA is deleted, the altered subsequent LTP reverts to its original behavior.[9] This dynamically reconfigurable mechanism helps to maintain synaptic performance within a dynamic range and keeps the larger neural network in an appropriate learning state. In addition, this increases the richness of synaptic plasticity and the developmental potential of neural networks, providing the basis for highly complex biological behaviors.

Note 2: Principles of Quantifying Synaptic Weight Values

Weight values in convolutional and fully connected layers can be quantized before mapping to device conductance. In order to quantize weights, you need to specify: the bit resolution of the quantized weights, and the range of values over which quantization will occur. The former is specified using the parameter weight bits. Setting this value

to 0 disables quantization, so floating point weights (or quantization weights) map directly to conductance. Other errors can then be applied to these conductances.

CrossSim provides an easy option to set the quantization range, using the weight percentile parameter; denote the value of this parameter as P. For a given layer's weight matrix W, find the maximum absolute weight: $W_{\text{absmax}} = \max(|W|)$. Then set the quantization range to $[-W_{\text{absmax}}, +W_{\text{absmax}}]$.

1 C. D. Yao, G. C. Wu, M. Q. Huang, W. Q. Wang, C. Zhang, J. X. Wu, H. W. Liu, B. Y. Zheng, J. L. Yi, C. G. Zhu, Z. L. Tang, Y. Z. Wang, M. Huang, L. Y. Huang, Z. W. Li, L. Xiang, D. Li, S. M. Li and A. L. Pan, *ACS Appl. Mater. Interfaces*, 2023, **15**, 23573-23582.

2 Z. Xu, Y. Ni, H. Han, H. Wei, L. Liu, S. Zhang, H. Huang and W. Xu, *Chinese Chemical Letters*, 2023, **34**.

3 Z. D. Luo, S. Q. Zhang, Y. Liu, D. W. Zhang, X. T. Gan, J. Seidel, Y. Liu, G. Q. Han, M. Alexe and Y. Hao, *ACS Nano*, 2022, **16**, 3362-3372.

4 S. Zhang, K. X. Guo, L. Sun, Y. Ni, L. Liu, W. L. Xu, L. Yang and W. T. Xu, *Adv. Mater.*, 2021, **33**, 9.

5 S. Kim, S. B. Jo, J. Kim, D. Rhee, Y. Y. Choi, D. H. Kim, J. Kang and J. H. Cho, *Adv. Funct. Mater.*, 2022, **32**, 10.

6 Y. Zhou, Y. S. Wang, F. W. Zhuge, J. M. Guo, S. J. Ma, J. L. Wang, Z. J. Tang, Y. Li, X. S. Miao, Y. H. He and Y. Chai, *Adv. Mater.*, 2022, **34**, 11.

7 Y. Zhang, C. H. Huang and K. Nomura, *Appl. Phys. Lett.*, 2022, **121**, 7.

8 W. C. Abraham, *Nat. Rev. Neurosci.*, 2008, **9**, 387-399.

9 Y. Y. Huang, A. Colino, D. K. Selig and R. C. Malenka, *Science (New York, N.Y.)*, 1992, **255**, 730-733.